

# **Exploring fibre orientation dispersion in the corpus callosum: Comparison of Diffusion MRI, Polarized Light Imaging and Histology**

*J. Mollink, M. Kleinnijenhuis, S. N. Sotiroopoulos, M. Cottaar, A. M. van Cappellen van Walsum, M. Pallebage Gamarallage, O. Ansorge, S. Jbabdi, K. L. Miller*

## **Purpose**

To investigate the microstructural correlates of diffusion-MR based estimates of fibre orientation dispersion through within tissue comparison against microscopy data.

## **Introduction**

While increasingly sophisticated models for diffusion-weighted MRI enable the reconstruction of crossing fibres in the brain, less attention has been paid to more subtle fibre architecture within a voxel such as fanning. These features have potential to improve current tractography paradigms or serve as markers of local fibre coherence<sup>1,2</sup>. We present a multimodal study comparing fibre orientation dispersion derived from a parametric dispersion model<sup>3</sup> in diffusion-MRI to equivalent models in microscopy images. Microscopic fibre orientations were derived from Polarized Light Imaging<sup>4</sup> (PLI) and histological myelin and glial staining, with the aim of understanding the microstructural features that correlate with the diffusion signal. Here, we use the corpus callosum (CC), a frequent test-bed for crossing fibre models, which is often assumed to be highly coherent pathway in which fibres are organized parallel. In fact, our results reveal a considerable amount of orientation dispersion, in agreement with previous literature<sup>5,6</sup>.

## **Methods**

Three 5 mm coronal slabs (S1-3) including the CC and the cingulate gyri were excised from formalin fixed brains. The pipelines for each sample can be found in Figure 1. **MRI:** Imaging was performed on a 9.4T preclinical Varian MR system using a diffusion-weighted spin echo sequence. 120 gradient directions (240 in sample S1) and 4 non-diffusion weighted images were acquired for two shells ( $b=2500, 5000$  s/mm<sup>2</sup>). Additional parameters: TR=2.4s, TE=29ms,  $\delta=6$ ms,  $\Delta=16$ ms and 0.4 mm

isotropic voxels. **PLI:** Samples were frozen before cutting them serially in 60 $\mu$ m sections. Sections were imaged with a polarizing microscope. Raw PLI images were acquired and processed according to existing protocols<sup>4</sup>.

**Histology:** Samples were imbedded in paraffin and cut at 6 $\mu$ m thickness. Sections were stained for proteolipidprotein (PLP, myelin marker) and glial-fibrillary-acidic-protein (GFAP, astroglial marker).

**Analysis:** The dispersion model was fitted to the  $b=5000$  s/mm<sup>2</sup> data that yielded a Bingham distribution for the anisotropic volume fraction of the diffusion signal. As PLI already provides high-resolution fibre orientation maps (FOM), a Bingham distribution could be directly fitted to local fibre orientation distributions. The eigenvalues of the Bingham distribution, reciprocally related to the amount of orientation dispersion, were converted to angles to produce orientation dispersion maps. PLI-sections from sample S2 were reconstructed to a volume (3D-PLI) by means of image-registration using the ANTs software as reported previously<sup>7,8</sup>. Dispersion profiles were extracted from 3D-PLI and MRI in the CC and correlated against each other. Finally, texture analysis revealed the sources of dispersion in CC after Fourier analysis of the histological images<sup>9</sup>.

## Results

Broadly similar patterns can be recognized in the orientation dispersion maps between diffusion imaging and PLI, with high dispersion in crossing fibre regions like the centrum semiovale and less dispersion in the CC (Figure 2). However, even a coherent white matter bundle as the CC is estimated to exhibit a considerable amount of dispersion. In S1-2 this seems to correspond to regional disorder in fibre orientation that can be observed in the PLI FOM's. In particular, S1-2 demonstrate a loss of coherence on the mid-line along with a "striping" appearance on the lateral aspects of the CC, while S3 appears much more coherent throughout. Regional quantification of these effects in the CC resulted in great correspondence for the dispersion profiles between 3D-PLI and the diffusion-derived estimates (Figure 3). Though there is discrepancy between the absolute values, relative dispersion profiles showed to correlate with each other. Figure 4 illustrates some of the sources that could contribute to fibre orientation dispersion estimated by MR models. In some regions of the CC there are significant glial cell processes with consistent orientation perpendicular to the main fibre orientation. The lateral areas with visible striping

patterns in PLI appear to have local fibre bundles running at large angles (~45 degrees) in close proximity.

## Discussion/conclusion

We present a multi-modal comparison of dispersion in the CC estimated from diffusion MRI and measured using microscopy data. A correlation was found in the CC in terms of relative dispersion profiles, although the dispersion angles were ~3 times larger in diffusion data, as estimated by a parametric dispersion model.

Sources of dispersion do not only originate from axons, but may also come from other structures in white matter. In addition, the current implementation of the dispersion model assumes a “stick-like” fibre response function. Having a cigar-like response function will result in lower dispersion and should be suitable for our data. Future work will aim to investigate if a simple but robust mapping between these modalities exists.

## References

1. Jbabdi S. & Johanssenberg H. (2010). Tractography, where do we go from here? *Brain Connectivity* 1:3:169-83
2. Zhang H. et al (2012). NODDI: practical *in vivo* neurite orientation dispersion and density imaging of the human brain. *Neuroimage*. 61:4:1000-16
3. Sotiroopoulos S.N. et al (2012). Ball and Rackets: Inferring fiber fanning from diffusion-weighted MRI. *Neuroimage* 60:2:1412-25
4. Axer M. et al (2011). High-resolution fiber tract reconstruction in the human brain by mean of three-dimensional polarized light imaging. *Frontiers in neuroinformatics*. 5:34
5. Budde M.D et al (2013). Quantification of anisotropy and fiber orientation in human brain histological sections. *Frontiers in integrative neuroscience*. 7:3
6. Mikula S, et al (2012). Staining and embedding the whole brain for electron microscopy. *Nature Methods*. 9:12:1198-201.
7. Adler D. et al (2014). Histology-derived volumetric annotation of the human hippocampal subfields in postmortem MRI. *Neuroimage* 84:505-23
8. Mollink J. et al (2015). Dentatorubrothalamic tract localization with postmortem MR diffusion tractography compared to histological 3D reconstruction. *Brain Structure and Function*.

9. Marquez J.P. (2006). Fourier analysis and automated measurement of cell and fiber angular orientation distributions. Int. Journal of Solids and Structures. 43:21:6413-23

## Figures

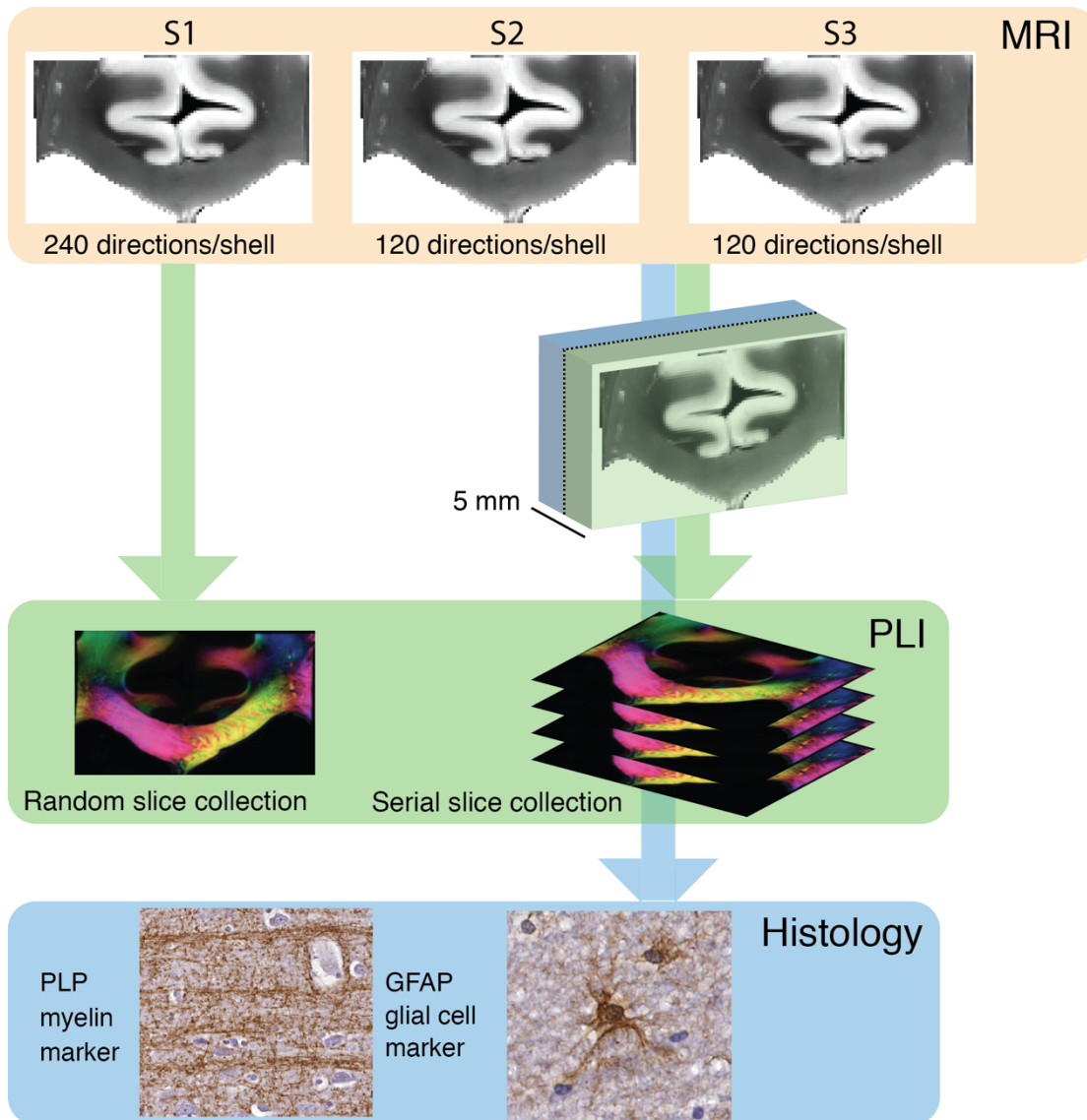


**Figure 1.** Imaging pipeline. No histological data was collected from S1. S2 and S3 were processed similarly, i.e. by splitting the sample after MR scanning in a PLI part and a histology part. Additionally, PLI slices for S2 and S3 were collected in a serial manner that allows 3D reconstruction.

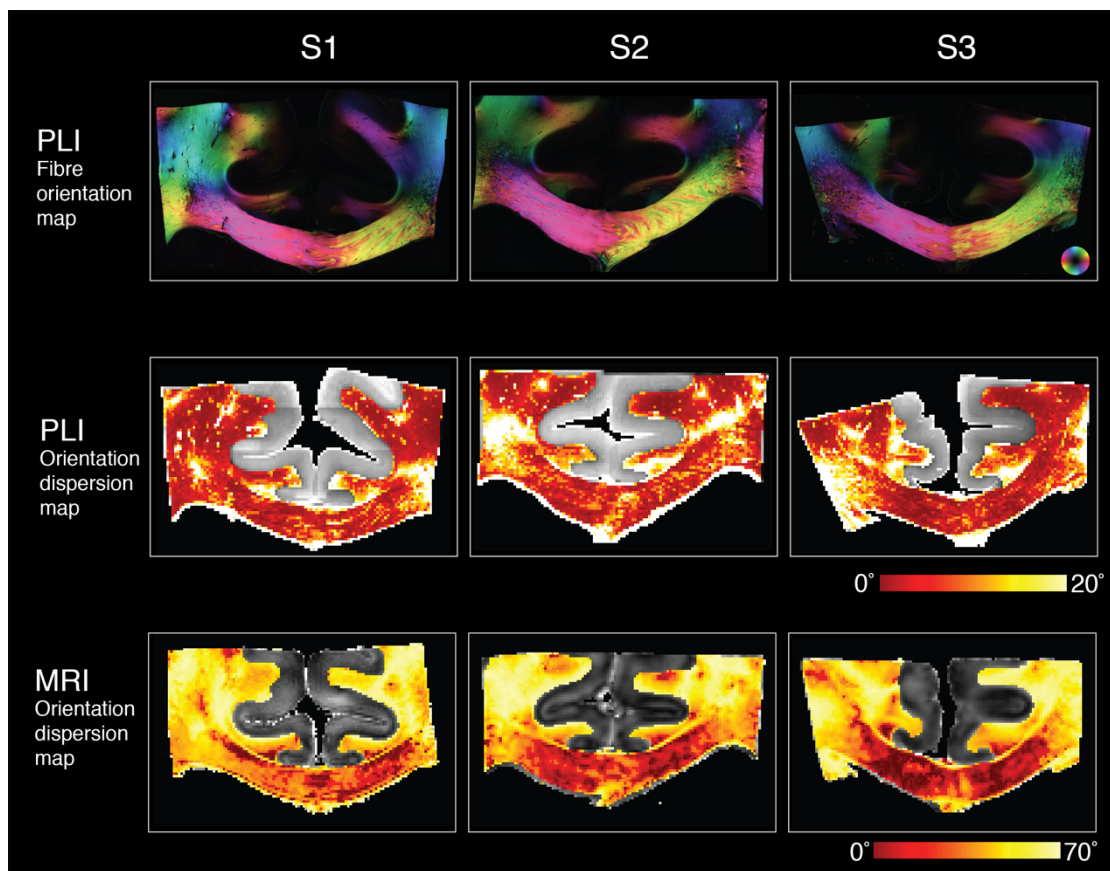


**Figure 2.** Fibre orientation and dispersion maps. PLI fiber orientation maps (PLI FOM) are shown in HSV colorspace, with the hue channel coding for the in plane fiber orientation. Dispersion maps represent the angular spread of fibres when 95% of the samples are included in the Bingham distribution.

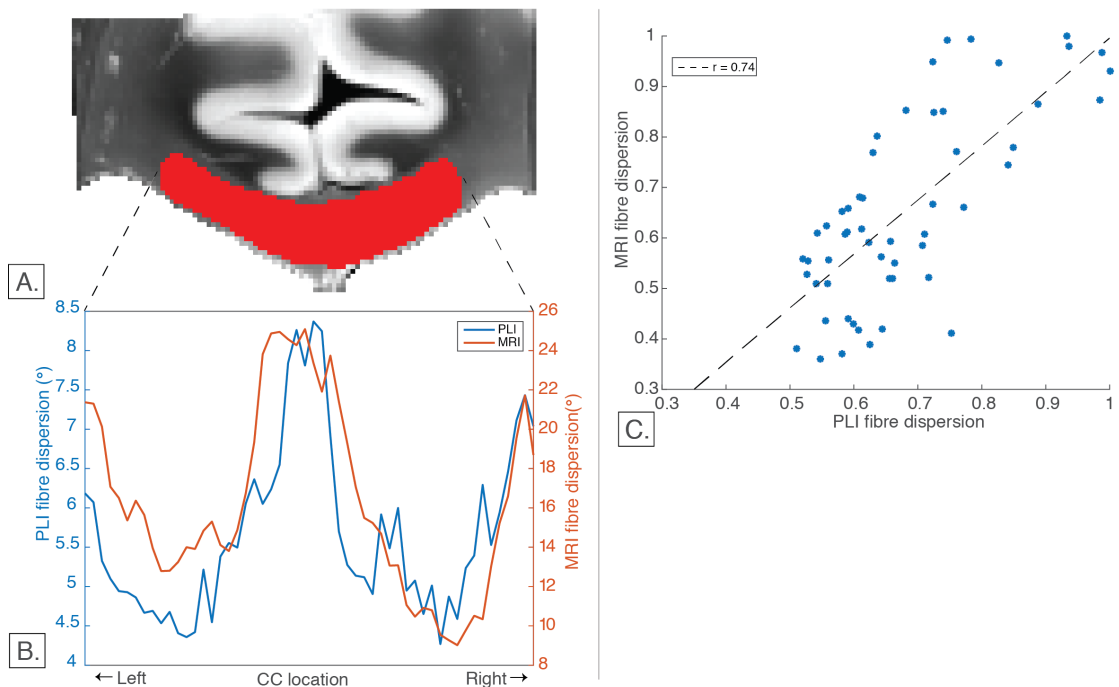


**Figure 3.** Fibre orientation dispersion in the corpus callosum demonstrated with PLI and diffusion MRI using a parametric dispersion model. A) Corpus callosum mask superimposed on transmittance map PLI. B) Fibre orientation dispersion profiles along the corpus callosum. C) Correlation between the relative orientation dispersion profiles.

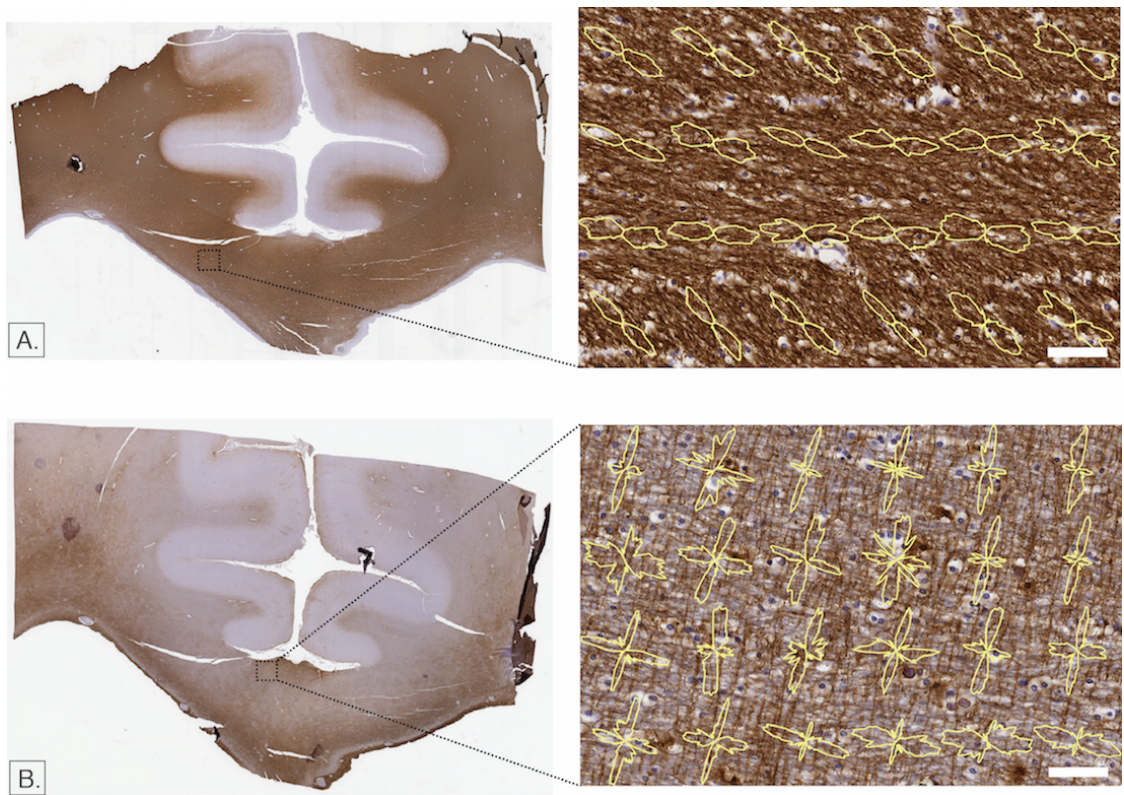


**Figure 4.** Sources of fibre orientation dispersion depicted in histological sections from S2. A) PLP stain. Within a small region in the CC, axonal orientations differ substantially from each other. B) GFAP stain. The close-up demonstrates fibre crossing of astrocyte processes with underlying axons. Scale-bar = 50  $\mu$ m